Heteroatom Chemistry
Volume 21, Number 7, 2010

NMR Study, Theoretical Calculations for Assignment of the *Z*- and *E*-Isomers, and Kinetics Investigation of Stable Phosphorus Ylides Involving a 2-Mercapto-4,6-dimethyl Pyrimidine

Mohammad Zakarianezhad, Sayyed Mostafa Habibi-Khorassani, Ali Ebrahimi, Malek Taher Maghsoodlou, and Hojjat Ghasempour

Department of Chemistry, University of Sistan and Baluchestan, P.O. Box 98135-674, Zahedan, Iran

Received 11 March 2010; revised 12 June 2010

ABSTRACT: *In the present work, NMR, theoretical, kinetics, and mechanism investigations were undertaken for a one-pot condensation reaction between 2-mercapto-4,6-dimethyl pyrimidine and dialkyl acetylenedicarboxylates in the presence of triphenyphosphine containing novel stable phosphorus ylides* **4a–c**. *Herein, theoretical calculations have been employed for assignment of the most stable isomers (*Z *or* E*) of phosphorus ylides* **4a,c** *by natural population analysis, atoms in molecules methods, and CHelpG keyword, in which* E-**4(a, c)** *are more stable forms as the majors. The* ^{1}H, ^{13}C, *and* ^{31}P *NMR data of these ylides are consistent with results obtained from theoretical calculations. In addition, kinetic investigation of new ylides was undertaken by ultraviolet spectrophotometry. Useful information was obtained from studies of the effect of solvent, structure of reactants (different alkyl groups within the dialkyl acetylenedicarboxylates), and also the concentration of reactants on the rate of reactions. The proposed mechanism was confirmed according to the obtained results and a steady-state approximation, and the first step* (k_2) *of the reaction was recognized as a rate-determining step on the basis of the experimental data.* © 2010 Wiley Periodicals, Inc. Heteroatom Chem 21:462–474, 2010; View this article online at wileyonlinelibrary.com. DOI 10.1002/hc.20632

INTRODUCTION

The synthesis of phosphorus ylides is an important reaction in organic chemistry because of the application of these compounds in the synthesis of organic products [1–29]. Several methods have been developed for the preparation of phosphorus ylides [10,11]. These ylides are usually prepared by treatment of a phosphonium salt with a base, and phosphonium salts are usually prepared from the phosphine and alkyl halide [2,3]. Phosphonium salts are also prepared by Michael addition of phosphorus to activated olefins [1]. The phosphonium salts are most often converted to the ylides by treatment with a strong base, though weaker bases can be used if the salt is acidic enough. Michael addition of phosphorus(III) compounds such as triphenylphosphine to acetylenic esters leads to reactive 1,3-dipolar intermediate betaines, which are not detected even at low temperatures [14]. These unstable species can be trapped by a protic reagent, ZH, such as methanol, amide, or imide, to produce various compounds, for example, ylides [4–29].

Correspondence to: Sayyed Mostafa Habibi-Khorassani; e-mail: smhabibius@yahoo.com.
Contract grant sponsor: University of Sistan and Baluchestan.

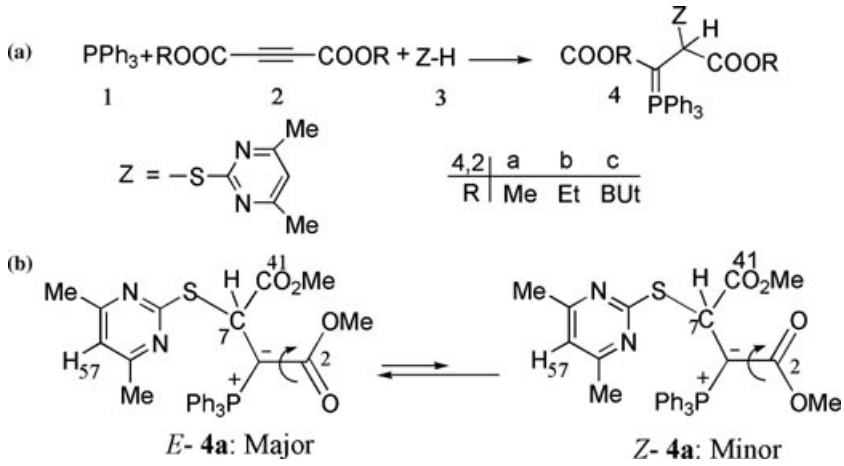

FIGURE 1 (a) The reaction between triphenylphosphine **1**, dialkyl acetylenedicarboxylate **2** (**2a, 2b**, or **2c**), and 2-mercapto-4,6-dimethyl pyrimidine **3** for generation of stable phosphorus ylides **4** (**4a, 4b**, or **4c**). (b) The two geometrical isomers *Z*-**4a** and *E*-**4a** (minor and major, respectively) of ylide **4a**.

These ylides usually exist as a mixture of the two geometrical isomers, although some ylides exhibit one geometrical isomer. Assignment of the stability of the two *Z*- and *E*- isomers is possible in phosphorus ylides by experimental methods, such as ^{1}H, ^{13}C NMR, IR spectroscopy, mass spectrometry, and elemental data analysis. For this reason, quantum mechanical calculation has been performed to gain a better understanding of the most important geometrical parameters and also relative energies of both the geometrical isomers.

MATERIALS AND METHODS

Quantum mechanical calculation has been performed by the Gaussian98 program and using the AIM2000 program packages. Di-*tert*-butylacetylenedicarboxylate, triphenylphosphine, and 2-mercapto-4,6-dimethyl pyrimidine were purchased from Fulka (Buchs, Switzerland) and used without further purification. All extra-pure solvents including 1,4-dioxane and ethyl acetate were obtained from Merck (Darmstadt, Germany). A Cary UV–vis spectrophotometer model Bio-300 with a 10-mm-light-path black quartz spectrophotometer cell was employed throughout the current work.

RESULTS AND DISCUSSION

Calculations

A facile synthesis of the reaction between triphenylphosphine **1**, dialkyl acetylenedicarboxylates **2**, and 2-mercapto-4,6-dimethyl pyrimidine **3** (as a SH-heterocyclic compound) was reported earlier [30] for the generation of phosphorus ylides **4a–c**, involving the two geometrical isomers such as *Z*- and *E*-isomers. The reaction is shown in Fig. 1. For assignment of the two *Z* and *E* isomers as a minor or major form in phosphorus ylides **4a,c** containing a 2-mercapto-4,6-dimethyl pyrimidine, first the *Z*- and the *E*-isomers were optimized for all ylide structures at the HF/6-31G(d,p) level of theory [31] by the Gaussian98 package program [32]. The relative stabilization energies in both geometrical isomers were calculated at the HF/6-31G(d,p) and B3LYP/6-311++G** levels. Atoms in molecules (AIM) [33], natural population analysis (NPA) methods, and CHelpG keyword at the HF/6-31G(d,p) level of theory were employed to gain a better understanding of the most geometrical parameters in both the *E*-**4(a, c)** and the *Z*-**4(a, c)** of phosphorus ylides. The theoretical results for ylide **4b** are nearly the same as those that were obtained for ylide **4a**, because the ylides **4a** and **4b** have very similar alkyl groups (methyl and ethyl, respectively); for this reason, calculations have been reported for just ylides **4a** and **4c**. The numbers of critical points and intramolecular hydrogen bonds have been recognized as well as the atoms that existed on the *Z*- and *E*-isomers. The results altogether reveal the effective factors on the stability of *Z* and *E* ylide isomers. The relative stabilization energies for the two [*Z*-**4(a, c)** and *E*-**4(a, c)**] isomers (see Figs. 2 and 3) are reported in Table 1; as can be seen, the *E*-**4a** and *E*-**4c** isomers are more stable than the *Z*-**4a** and *Z*-**4c** forms (1.00 and 1.27 kcal/mol, respectively) at the B3LYP level. In addition, J_{x-y}, the values of proton and carbon coupling constants, and also chemical shifts (δ^{H}_{iso}, δ^{C}_{iso}) have been calculated at the mentioned level using SPINSPIN keyword.

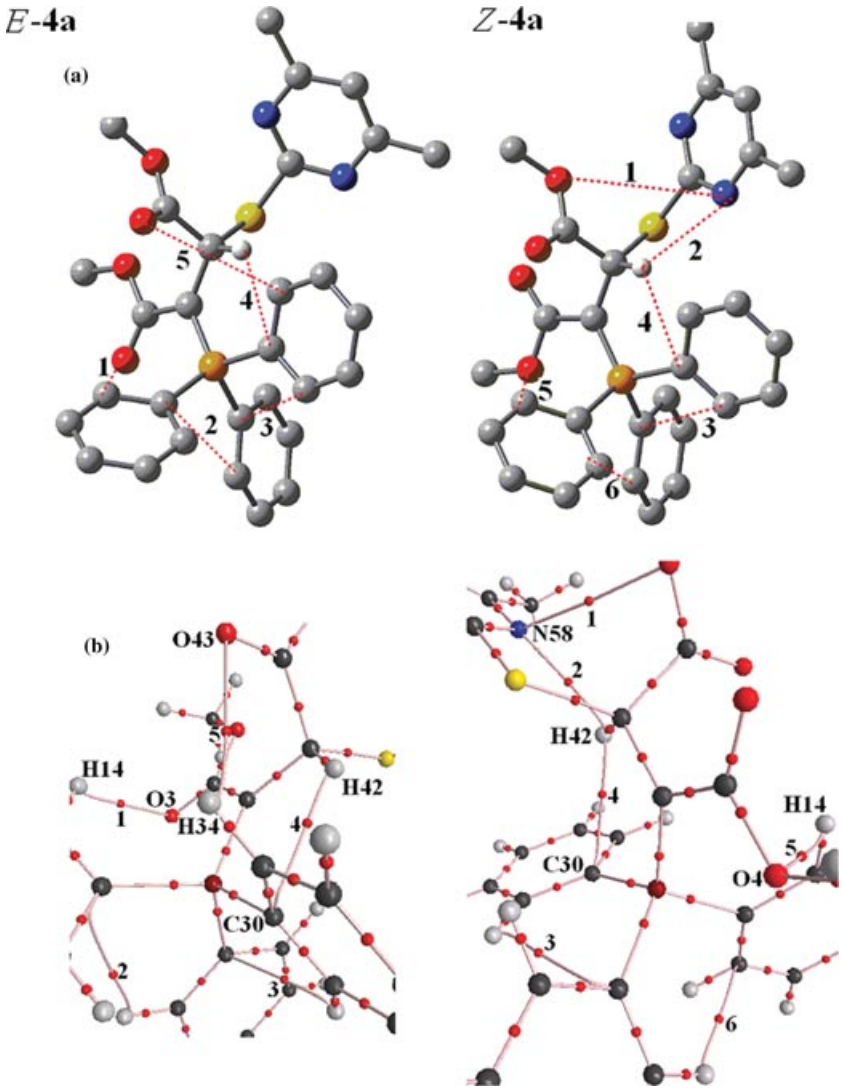

FIGURE 2 (a) Intramolecular hydrogen bonds (dotted lines) in the two *E*-**4a** and *Z*-**4a** geometrical isomers of stable ylide **4a**. (b) Partial molecular graphs, including intramolecular hydrogen bond critical points (BCPS) for the two rotational isomers such as *E*-**4a** and *Z*-**4a**. Small red spheres and lines correspond to BCPS bond paths, respectively.

Further investigation was undertaken to determine more effective factors in the stability of the two *Z*- and *E*- isomers, on the basis of AIM calculations at the HF/6-31G(d,p) level of theory by the AIM2000 program package [34]. In recent years, AIM theory has often been applied in the analysis of H bonds. In this theory, the topological properties of the electron density distribution are derived from the gradient vector field of the electron density $\nabla\rho(r)$ and on the Laplacian of the electron density $\nabla^2\rho(r)$. The Laplacian of the electron density, $\nabla^2\rho(r)$, identifies regions of space wherein the electronic charge is locally depleted $[\nabla^2\rho(r) > 0]$ or built up $[\nabla^2\rho(r) < 0]$ [33]. Two interacting atoms in a molecule form a critical point in the electron density, where $\nabla\rho\ (r) = 0$, called the bond critical point (BCP). The values of the charge density and its Laplacian at these critical points give useful information regarding the strength of the H bonds [34]. The ranges of $\rho(r)$ and $\nabla^2\rho(r)$ are 0.002–0.035 e/a_0^3 and 0.024–0.139 e/a_0^5, respectively, if H bonds exist [35]. The AIM calculation indicates intramolecular hydrogen bond critical points (H-BCP) for the two *Z*-**4(a, c)** and *E*-**4(a, c)** isomers. Intramolecular H-BCPs along with partial molecular graphs for the two rotational isomers are shown in Figs. 2 and 3 (dotted lines). The most important geometrical parameters involving some H bonds (bond length and their relevant bond angle) are reported in Table 2. The electron densities $(\rho) \times 10^3$, Laplacian of electron density $\nabla^2\rho(r) \times 10^3$, and energy density

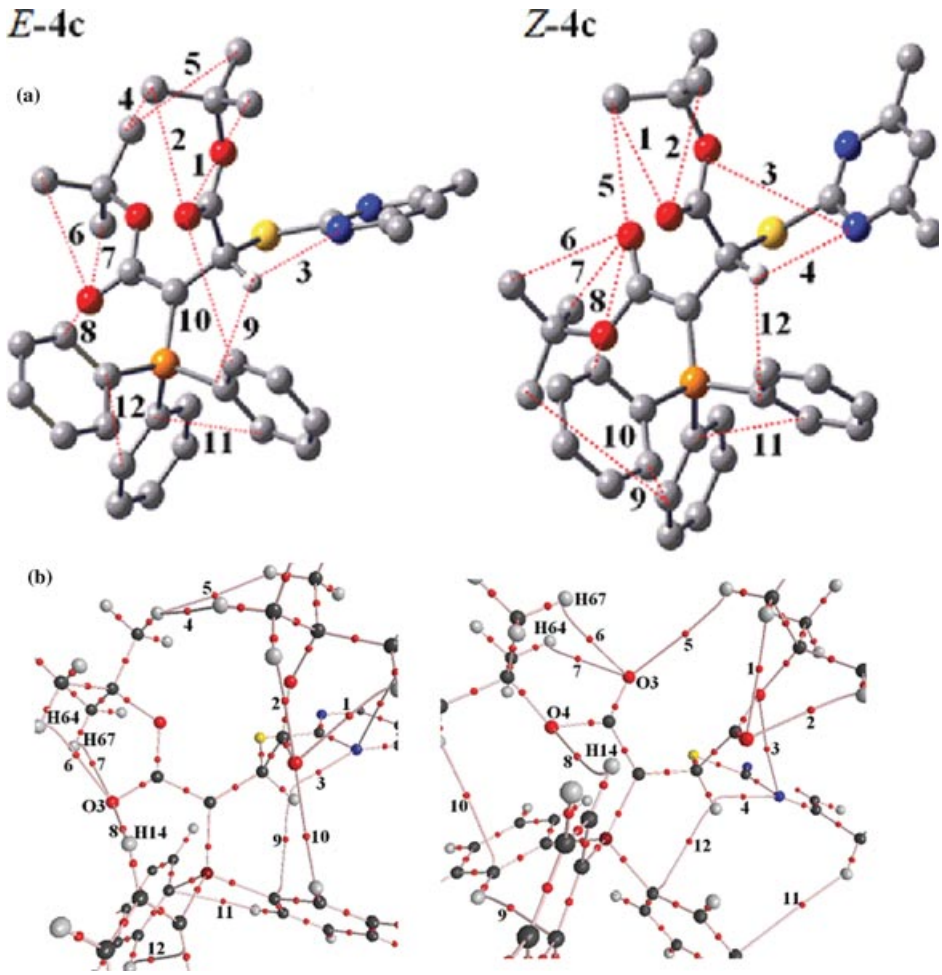

FIGURE 3 (a) Intramolecular hydrogen bonds (dotted lines) in the two *E*-**4c** and *Z*-**4c** geometrical isomers of stable ylide **4c**. (b) Partial molecular graphs, including intramolecular hydrogen bond critical points (BCPS) for the two rotational isomers such as *E*-**4c** and *Z*-**4c**. Small red spheres and lines correspond to BCPS bond paths, respectively.

$-H(r) \times 10^4$ are also reported in Tables 3 and 4. A negative total energy density at the BCP reflects a dominance of potential energy density, which is the consequence of an accumulated stabilizing electronic charge [36]. The numbers of hydrogen bonds in both categories (*E*-**4a** and *Z*-**4a**) and (*E*-**4c** and *Z*-**4c**) are 5 and 6 and 12 and 12, and the values of ρ and $\nabla^2\rho(r) \times 10^3$ for them are in the ranges 0.003–0.012 and 0.006–0.013 e/a_0^3, 0.002–0.014 and 0.002–0.013 e/a_0^3, 14.56–45.48 and 26.36–57.76 e/a_0^5, and 7.60–58.84 and 8.88–57.16 e/a_0^5, respectively. In addition, the Hamiltonians $[-H(r) \times 10^4]$ are in the ranges 8.60–17.80 and 5.80–22.60 au and 5.00–21.30 and 4.80–21.40 au, respectively (see Tables 3 and 4). These HBs show $\nabla^2\rho(r) > 0$ and $H(r) < 0$, which according to the classification of Rozas et al. [37] are medium-strength hydrogen bonds. Although dipole moment in *E*-**4a** (5.42 D) is less than that in *Z*-**4a** (7.00 D) and appears to be an effective factor of *E*-**4a** stability, the value of $-H_{tot}$ in *E*-**4a** (67.9 au) is less than in *Z*-**4a** (88.6 au), an important factor in the instability of *E*-**4a** (Table 5). It seems that the *E*-**4a** stability stems from the two opposite factors (dipole moment and total Hamiltonian) in which the influence of dipole moment is superior to that of total Hamiltonian, resulting in a slight relative stability in *E*-**4a** (1 kcal/mol in comparison with the *Z*-**4a** isomers). This is in good agreement with the experimental results [30] based upon the ^{1}H, ^{13}C, and ^{31}P NMR data with a slightly more experimental abundance percentage of 59 for *E*-**4a**. The total value of the total Hamiltonian ($-H_{tot}$ ($=\sum -H(r) \times 10^4$)) in both the *E*-**4c** and *Z*-**4c** isomers is approximately the same (153 and 152 au, respectively) but the dipole moment in *E*-**4c** (5.55 D) is less than in *Z*-**4c** (6.96 D); in fact the latter factor accounts as a lone factor on relative stability of *E*-**4c** (1.27 kcal/mol in comparison with *Z*-**4c**). This difference in stabilization energy is also too low in which the observation of two *E*-**4c** and *Z*-**4c** is reasonable. Herein, there is a

TABLE 1 Relative Energy (kcal/mol) for the *Z*- and *E*-Isomers of Ylides **4a** and **4c**, Obtained at HF/6-31G (d,p) and B3LYP/6-311++G(d,p) Levels

Geometrical Isomer	*HF*	*B3LYP*
Z-**4a**	1.50	1.00
E-**4a**	0.00	0.00
Z-**4c**	0.47	1.27
E-**4c**	0.00	0.00

good agreement between the results obtained from the ^{1}H, ^{13}C,^{31}P NMR data with a slightly more experimental abundance percentage of 56 for *E*-**4c**.

Also, the charges on different atoms, which are calculated by AIM, NPA methods, and CHelpG keyword at HF/6–31G(d,p) level, are reported in Table 6 for the two *Z*- and *E*-isomers of ylides **4a** and **4c**. There is a good agreement among the results in the three methods.

The individual chemical shifts have been characterized by NMR calculations at the mentioned level. The total spin–spin coupling constant is the sum of four components: the paramagnetic spin-orbit (PSO), diamagnetic spin-orbit (DSO), Fermi-contact (FC), and spin-dipole (SD) terms. The value of chemical shifts (δ) and coupling constants (J_{x-y}) are reported in Tables 7–10. As can be seen, there is a good agreement between both the experimental [30] and theoretical chemical shifts (δ) and coupling constants (J_{x-y}). In the present work, molecular structures of ylides **4a–c** involving four large atoms such as sulfur, phosphorus, and two nitrogen atoms are huge, with large numbers of other atoms (C, H); for this reason, a basis set higher than HF/6-31G(d, p) is impossible in a higher performance for obtaining more accurate calculations. This limitation results in a difference between both the experimental and theoretical coupling constants and chemical shifts in some functional groups.

TABLE 3 Values of $a = \rho \times 10^3$, $b = \nabla^2\rho \times 10^3$, and $c = -H(r) \times 10^4$ for the *Z*-**4a** and *E*-**4a** Isomers of Ylide **4a** Calculated at the Hydrogen Bond Critical Points

E	*a*	*b*	*c*	*Z*	*a*	*b*	*c*
1	12.15	45.48	9.50	1	6.90	26.36	5.80
2	9.22	32.08	15.10	2	13.41	57.76	22.60
3	9.60	36.80	17.80	3	8.99	32.12	15.50
4	11.89	42.00	16.90	4	10.65	39.04	17.20
5	3.30	14.56	8.60	5	6.73	28.92	12.60
				6	9.71	34.16	14.90

All values are in atomic units.

TABLE 4 Values of $a = \rho \times 10^3$, $b = \nabla^2\rho \times 10^3$, and $c = -H(r) \times 10^4$ for the *Z*-**4c** and *E*-**4c** Isomers of Ylide **4c** Calculated at the Hydrogen Bond Critical Points

E	*A*	*b*	*C*	*Z*	*a*	*b*	*c*
1	12.05	46.60	13.00	1	11.85	46.32	13.50
2	12.34	47.68	13.00	2	11.75	45.28	12.50
3	14.29	58.84	21.30	3	6.31	25.48	6.70
4	2.50	8.88	5.90	4	13.72	57.16	21.40
5	2.14	7.60	5.00	5	3.15	13.92	7.90
6	13.05	49.64	12.10	6	13.13	49.76	11.90
7	12.89	48.96	12.20	7	12.67	48.36	12.40
8	11.60	44.36	10.70	8	6.98	29.92	12.80
9	11.90	42.20	16.80	9	9.72	34.48	15.00
10	5.65	22.84	10.10	10	2.74	8.88	4.80
11	9.78	36.96	17.60	11	9.12	33.48	16.20
12	9.16	31.68	14.90	12	11.07	40.36	17.30

All values are in atomic units.

Kinetics Studies

To gain further insight into the reaction mechanism between triphenylphosphine **1**, dialkyl acetylenedicarboxylates **2**, and 2-mercapto-4,6-dimethyl pyrimidine **3** (as a SH-heterocyclic compound) for the generation of phosphorus ylides 4**a–c**, a kinetic study of the reactions was undertaken by the UV spectrophotometric technique. The synthesis of these reactions

TABLE 2 Most Important Geometrical Parameters Corresponding to H Bonds (Bond Lengths and Their Relevant Angles) for the Two *Z* and *E* Isomers in Ylides **4a** and **4c**

	*E-**4a***	*Z-**4a***	*E-**4c***	*Z-**4c***
$C_{31}H_{34}\cdots O_{43}$	2.98[a] (129.46)[b]			
$C_{10}H_{14}\cdots O^{c}_{3(4)}$	2.39 (124.91)	2.74 (109.33)	2.42 (121.98)	
$C_7H_{42}\cdots C_{30}$	2.53 (118.17)	2.60 (114.47)		
$C_7H_{42}\cdots N_{58}$		2.48 (101.46)		
$C_{62}H_{64}\cdots O_3$			2.42 (110.97)	2.43 (111.56)
$C_{66}H_{67}\cdots O_3$			2.43 (111.70)	2.41 (112.03)
$C_{78}H_{80}\cdots O_{43}$				2.47 (111.19)

Bond lengths are in angstroms, and bond angles are in degrees.
[a]Bond length.
[b]Bond angle.
[c]It is relevant to the *Z* isomer.

TABLE 5 Most Important Geometrical Parameters Involving the Value of $-H_{tot}$ (in au), Dipole Moment (in D), and the Number of Hydrogen Bonds for the Two *Z*- and *E*-Isomers of Ylides **4a** and **4c**

Geometrical Isomer	$-H_{tot}$ *(au)*	*Dipole Moment (D)*	*Number of Hydrogen Bonds*
E-**4a**	67.9	5.42	5
Z-**4a**	88.6	7.00	6
E-**4c**	153	5.55	12
Z-**4c**	152	9.96	12

TABLE 7 Selected ^{1}H NMR Chemical Shift (δ in ppm) and Coupling Constants (J in Hz) for Some Functional Groups in the *E*-**4a** Isomer as a Major Form

Groups	δ^H *(ppm)*	J_{PH} *(Hz)*
6H, 2s, 2 CO_2Me	3.76[a] and 3.81[a] (3.50 and 3.53)[b]	
6H, s, $ArMe_2$	2.15 (2.24)	
1H, s, Ar-H[57]	6.68 (6.25)	
15H, m, $3C_6H_5$	7.31–7.75 (7.24–7.82)	
1H, d, P=C—CH	4.88 (3.89)	19.70[a] (19.69)[b]

[a]Experimental data in accord with the results reported in the literature [30].
[b]Theoretical data.

TABLE 8 Selected ^{1}H NMR Chemical Shift (δ in ppm) and Coupling Constants (J in Hz) for Some Functional Groups in the *Z*-**4a** Isomer as a Minor Form

Groups	δ^H *(ppm)*	J_{PH} *(Hz)*
6H, s, $ArMe_2$	2.31[a] (2.36)[b]	
6H, 2s, 2 CO_2Me	3.67 and 3.74 (3.32 and 3.64)	
1H, s, Ar-H[57]	6.75 (6.23)	
15H, m, $3C_6H_5$	7.31–7.75 (7.36–7.92)	
1H, d, P=C—CH	4.96 (3.85)	18.10[a] (17.67)[b]

[a]Experimental data in accord with the results reported in the literature [30].
[b]Theoretical data.

has been reported earlier [30]. First, it was necessary to find the appropriate wavelength to follow the kinetic study of the reaction. For this purpose, in the first experiment, 3×10^{-3} M solution of compounds **1, 2c**, and **3** was prepared in 1,4-dioxane as solvent. An approximately 3-mL aliquot from each reactant was pipetted into a 10-mm-light-path quartz spectrophotometer cell, and the relevant spectra were recorded over the wavelength range 190–400 nm. Figures 4–6 show the UV spectra of compounds **1, 2c**, and **3**, respectively. In a second experiment, a 1-mL aliquot from the 3×10^{-3} M solutions of each compound of **1** and **3** was pipetted first into a quartz spectrophotometer cell (as there is no reaction between them); later a 1-mL aliquot of the 3×10^{-3} M solution of reactant **2c** was added to the mixture, and the reaction was monitored by recording scans of the entire spectra every 10 min over the whole reaction time at ambient temperature. The UV spectra shown in Fig. 7 are typical. From this, the appropriate wavelength was found to be 410 nm (corresponding mainly to 2-mercapto-4,6-dimethyl pyrimidine **3**). At this wavelength, compounds **4, 2c**, and **1** have relatively no absorbance value. This then provided the opportunity to fully investigate the kinetics of the reaction between triphenylphosphine **1**, di-*tert*-butyl acetylenedicarboxylate **2c**, and 2-mercapto-4,6-dimethyl pyrimidine **3** at 410 nm in the presence of 1,4-dioxane as solvent. Since the spectrophotometer cell of the UV instrument had a 10-mm-light-path cuvette, the UV–vis spectra of compound **4c** were measured over the concentration range $2 \times 10^{-4}\text{M} \leq M_{4c} \leq 10^{-3}$ M to check for a linear relationship between absorbance values and concentrations. With the suitable concentration range and wavelength identified, the following procedure was employed.

For each kinetic experiment, first a 1-mL aliquot from each freshly made 3×10^{-3} M solution of

TABLE 6 Charges on Different Atoms for the Two *E*- and *Z*-Isomers in Ylides **4a** and **4c**, Calculated at HF/6-31G(d,p) Theoretical Level

Number of Atoms	*Z-**4a***	*E-**4a***	*Z-**4c***	*E-**4c***
C1	−0.80[a] (−0.37)[b] (−0.89)[c]	−0.73 (−0.52) (−0.87)	−0.78 (−0.36) (−0.89)	−0.74 (−0.56) (−0.87)
C2	1.85 (0.92) (0.96)	1.86 (0.93) (0.95)	1.87 (0.89) (0.96)	1.86 (0.94) (0.96)
C7	0.26 (−0.04) (−0.45)	0.24 (−0.01) (−0.45)	0.29 (0.06) (−0.44)	0.28 (0.24) (−0.45)
O3	−1.39 (−0.66) (−0.76)	−1.41 (−0.73) (−0.80)	−1.41 (−0.63) (−0.78)	−1.41 (−0.73) (−0.81)
O4	−1.29 (−0.48) (−0.66)	−1.26 (−0.34) (−0.64)	−1.28 (−0.63) (−0.69)	−1.24 (−0.57) (−0.67)
P6	3.25 (0.04) (1.87)	3.24 (0.18) (1.88)	3.24 (0.06) (1.87)	3.24 (0.14) (1.88)

[a]Calculated by the AIM method.
[b]Calculated by the CHelpG Keyword.
[c]Calculated by the NPA method.

TABLE 9 Selected ^{13}C NMR Chemical Shift (δ in ppm) and Coupling Constants (J in Hz) for Some Functional Groups in the *E*-**4a** Isomer as a Major Form

Groups	δ^C *(ppm)*	J_{PC} *(Hz)*
d, C^{41}=O	169.31[a] (169.32)[b]	
d, C_{ortho}	132.49 (134.11)	9.90[a] (10.34)[b]
d, C_{ipso}	124.77 (127.76)	92.20 (91.10)
S, $ArMe_2$	22.41 (23.53)	
d, C_{meta}	127.38 (126.26)	12.00 (8.52)
d, C_{para}	130.61 (132.15)	
2s, 2Ome	49.35 and 51.28 (46.10 and 46.99)	
d, P—C=C^2	171.93 (167.32)	10.70 (10.12)
s, 2Cme	164.84 (169.54)	
d, P—C—C^7H	48.44 (44.55)	
CH^{57}	113.45 (107.57)	

[a]Experimental data in accord with the results reported in the literature [30].
[b]Theoretical data.

TABLE 10 Selected ^{13}C NMR Chemical Shift (δ in ppm) and Coupling Constants (J in Hz) for Some Functional Groups in the *Z*-**4a** Isomer as a Minor Form

Groups	δ^H *(ppm)*	J_{PHz} *(Hz)*
d, C^{41}=O	168.14[a] (169.42)[b]	
d, C_{ortho}	132.49 (132.79)	9.90[a] (10.64)[b]
d, C_{meta}	127.27 (126.71)	10.80 (8.40)
d, C_{ipso}	125.44 (127.04)	91.90 (90.55)
d, C_{para}	130.70 (132.12)	
S, $ArMe_2$	22.41 (23.55)	
2s, 2Ome	47.89 and 51.28 (45.31 and 47.10)	
d, P—C—C^7H	49.27 (45.74)	
CH^{57}	113.31 (107.38)	
d, P—C=C^2	171.79 (164.00)	10.50 (6.88)
s, 2Cme	164.77 (169.27)	

[a]Experimental data in accord with the results reported in the literature [30].
[b]Theoretical data.

compounds **1** and **3** in 1,4-dioxane was pipetted into a quartz cell, and then a 1-mL aliquot of the 3×10^{-3} M of solution of the reactant **2c** was added to the mixture, keeping the temperature at 15.0°C. The reaction kinetics was followed by plotting UV absorbance against time. Figure 8 shows the absorbance change (dotted line) versus time for the 1:1:1 addition reaction between compounds **1, 2c**, and **3** at 15.0°C. The infinity absorbance (A_∞), that is, the absorbance at reaction completion, can be observed from Fig. 8 at $t = 200$ min. With respect to this value, zero, first, or second curve fitting could be drawn automatically for the reaction by the software [38] associated with the UV instrument. Using the original experimental absorbance versus time data

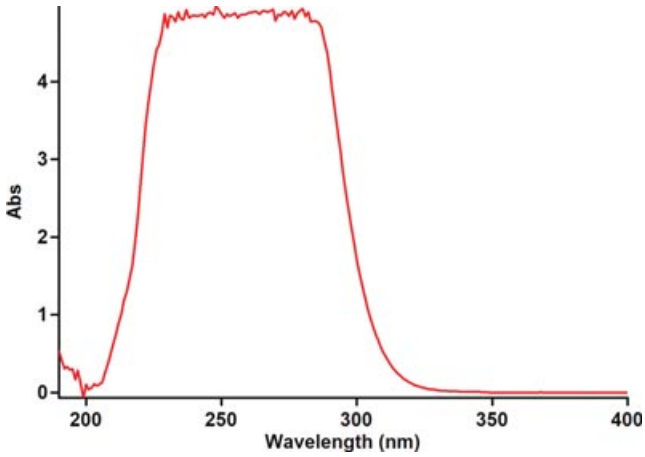

FIGURE 4 UV spectrum of 10^{-3} M of triphenylphosphine **1** in 1,4-dioxane.

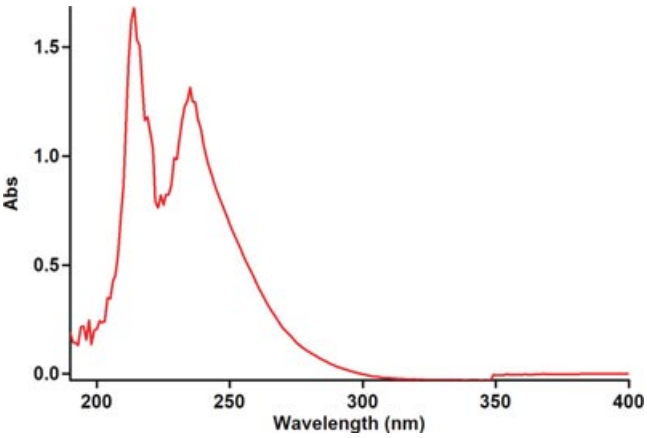

FIGURE 5 UV spectrum of 10^{-3} M of di-*tert*-butyl acetylenedicarboxylate **2c** in 1,4-dioxane.

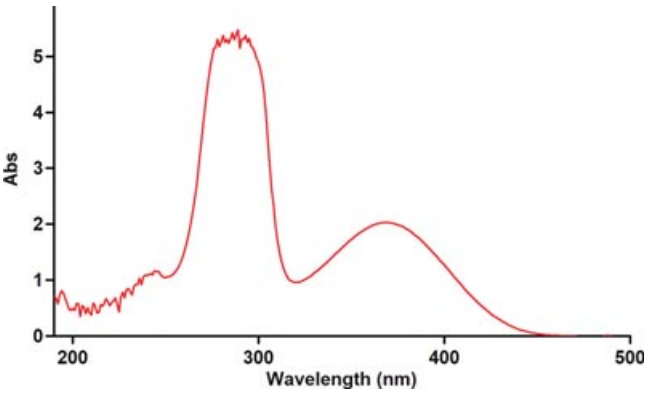

FIGURE 6 UV spectrum of 10^{-3} M of 2-mercapto-4,6-dimethyl pyrimidine **3** in 1,4-dioxane.

provided a second-order fit curve (full line) that fits exactly the experimental curve (dotted line) as shown in Fig. 9. Thus, the reaction between triphenylphosphine **1**, di-*tert*-butyl acetylenedicarboxylate **2c**, and

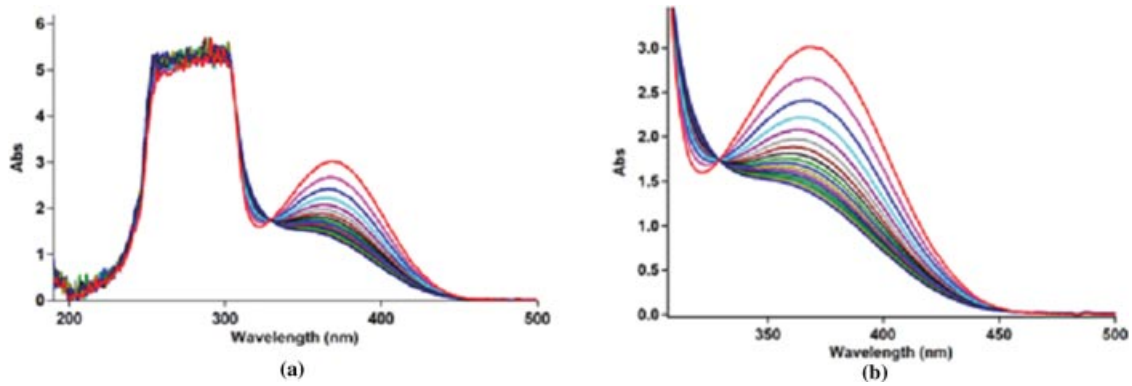

FIGURE 7 (a) UV spectra of the reaction between **1, 2c**, and **3** with 10^{-3} M concentration of each compound as reaction proceeds in 1,4-dioxane with 10-mm-light-path cell. (b) Expanded section of the UV spectra over the wavelength range 310–500 nm.

3 follows second-order kinetics. The second-order rate constant (k_2) is then automatically calculated using a standard equation [38] within the program at 15.0°C. It is reported in Table 11.

Furthermore, kinetic studies were carried out using the same concentration of each reactant in the continuation of experiments with concentrations of 5×10^{-3} M and 7×10^{-3} M, respectively. As expected, the second-order rate constant was independent of the concentration and its value was the same as in the previous experiment. In addition, the overall order of reaction was also 2.

Effect of Solvents and Temperature

To determine the effect of change in temperature and solvent environment on the rate of reaction, it was elected to perform various experiments at different temperatures and solvent polarities but otherwise under the same conditions as for the previous experiment. For this purpose, ethyl acetate with 6 dielectric constant was chosen as a suitable solvent because it not only could dissolve all compounds but also did not react with them. The effects of solvents and temperature on the rate constant are presented in Table 11. The results show that the rate of reaction in each case was increased at higher temperatures. In addition, the rate of reaction between **1, 2c**, and **3** was accelerated in a higher dielectric constant environment (ethyl acetate) in comparison with a lower dielectric constant environment (1,4-dioxane) at all temperatures investigated. In the temperature range studied, the dependence of the second-order rate constant ($\ln k_2$) of the reactions on the reciprocal temperature is consistent with the Arrhenius equation, giving activation energy of reaction between

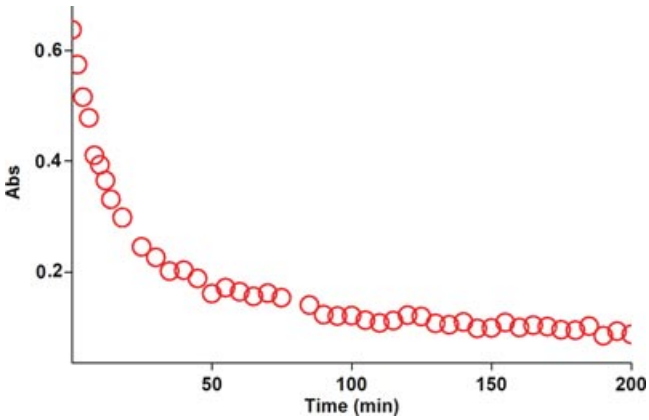

FIGURE 8 Experimental absorbance changes against time at 410 nm for the reaction between compounds **1, 2c**, and **3** at 15.0°C in 1,4-dioxane.

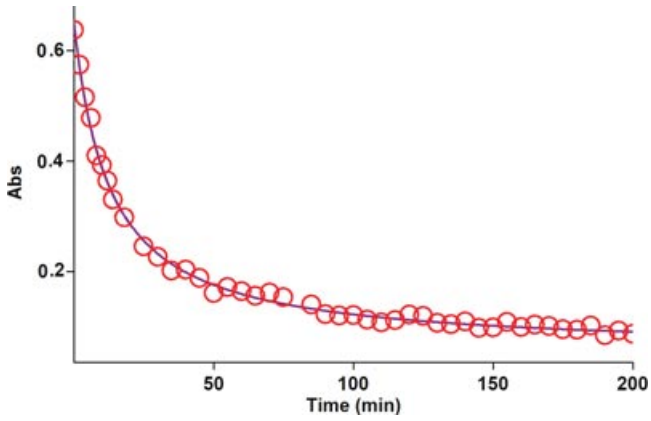

FIGURE 9 Second-order fit curve (solid line) accompanied by the original experimental curve (circles) for the reaction between compounds **1, 2c**, and **3** at 410 nm and 15.0°C in 1,4-dioxane.

TABLE 11 Values of Overall Second-Order Rate Constant for the Reaction Between **1, 2c**, and **3** in the Presence of Solvents Such As 1,4-Dioxane and Ethyl Acetate, Respectively, at All Temperatures Investigated

		$k_2(M^{-1}\ min^{-1})$			
Solvent	ε	*15.0°C*	*20.0°C*	*25.0°C*	*30.0°C*
1,4-Dioxane	2	73.5	92.7	109.9	131.9
Ethyl acetate	6	114.9	131.2	156.4	184.6

1, 2c, and **3** (27.9 kJ/mol) from the slope shown in Fig. 10.

Effect of Concentration

To determine the reaction order with respect to triphenylphosphine **1** and dialkyl acetylenedicarboxylate **2** (**2c**) in the next experiments, all kinetic studies were carried out in the presence of excess **3**. Under this condition, the rate equation may therefore be expressed as

$$\text{Rate} = k_{\text{obs}}\,[1]^{\alpha}\,[2]^{\beta} \quad k_{\text{obs}} = k_2\,[3]^{\gamma} \quad \text{or} \quad \ln\,k_{\text{obs}} = \ln\,k_2 + \gamma\,\ln[3] \tag{1}$$

In this case, 3×10^{-2} M of **3** instead of 3×10^{-3} M using the original experimental absorbance versus time data provides a second-order fit curve (solid line) against time at 410 nm, which exactly fits the experimental curve. The value of rate constant was the same as that obtained from the previous experiment (3×10^{-3} M). Repetition of the experiments with 5×10^{-2} M and 7×10^{-2} M of **3** gave, separately, the same fitted curve and rate constant. In fact, the experimental data indicated that the observed pseudo-second-order rate constant (k_{obs}) was

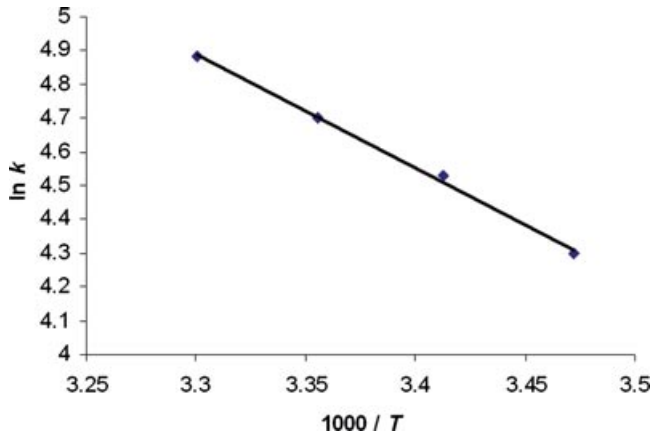

FIGURE 10 Dependence of the second-order rate constant (ln k_2) on reciprocal temperature for the reaction between compounds **1, 2c**, and **3** measured at wavelength 410 nm in 1,4-dioxane in accordance with the Arrhenius equation.

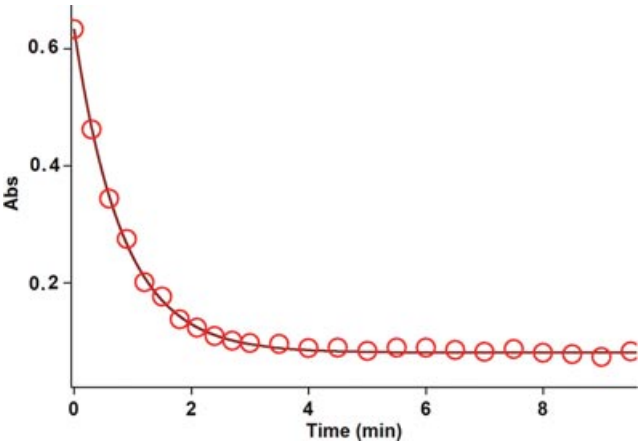

FIGURE 11 Pseudo-first-order fit curve (solid line) for the reaction between **3** and **2c** in the presence of an excess of **1** (10^{-2} M) at 410 nm and 15.0°C in 1,4-dioxane.

equal to the second-order rate constant (k_2); this is possible when γ is zero in Eq. (1). It appears, therefore, that the reaction is zero and second order with respect to **3** (SH-acid) and the sum of **1** and **2** (**2a**) ($\alpha + \beta = 2$), respectively.

To determine the reaction order with respect to dialkyl acetylenedicarboxylate **2** (**2c**), the next experiment was performed in the presence of an excess of **1** (rate $= k'_{\text{obs}}\,[3]^{\gamma}\,[2]^{\beta}$, $k'_{\text{obs}} = k_2\,[1]^{\alpha}$ (Eq. 2)). The original experimental absorbance versus time data provides a pseudo-first-order fit curve at 410 nm, which exactly fits the experimental curve (circles) as shown in Fig. 11.

As a result, since $\gamma = 0$ (as determined previously), it is reasonable to accept that the reaction is first order with respect to compound **2** (**2c**) ($\beta = 1$). Because the overall order of reaction is 2 ($\alpha + \beta + \gamma = 2$), it is obvious that $\alpha = 1$ and the order of triphenylphosphine **1** must be equal to one. This observation was also obtained for reactions between **1, 2b**, and **3** and 1, **2a**, and **3**. On the basis of the above results, a simplified proposed reaction mechanism is shown in Fig. 12.

The experimental results indicate that the third step (rate constant k_3) is possibly fast. In contrast, it may be assumed that the third step is the rate-determining step for the proposed mechanism. In this case, the rate law can be expressed as follows:

$$\text{Rate} = k_3[I_1][3] \tag{3}$$

The steady-state assumption can be employed for $[I_1]$, which is generated by the following equation:

$$[I_1] = \frac{k_2[1][2]}{k_{-2} + k_3[3]}$$

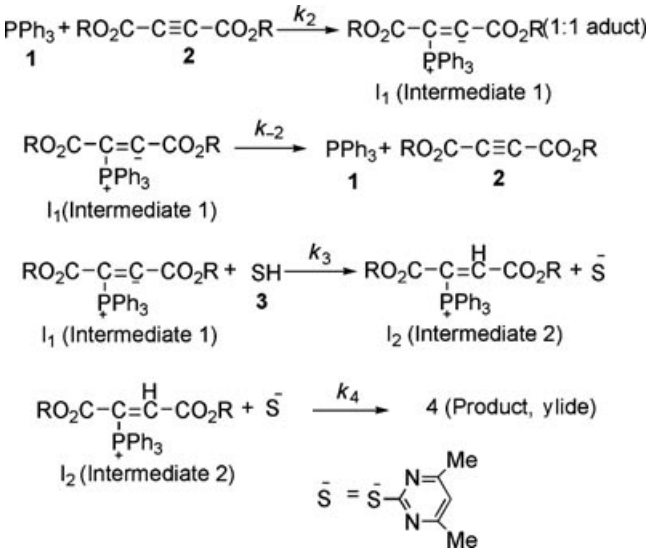

FIGURE 12 Proposed mechanism for the reaction between **1, 2** (**2a, 2b**, or **2c**), and **3** for the generation of phosphorus ylides **4a–c**.

The value of $[I_1]$ can be replaced in Eq. (3) to obtain the equation

$$\text{Rate} = \frac{k_2 k_3 [1][2][3]}{k_{-2} + k_3 [3]}$$

Since it was assumed that k_3 is relevant to the rate-determining step, it is reasonable to make the following assumption:

$$k_{-2} \gg k_3\,[3]$$

So the rate law becomes

$$\text{Rate} = \frac{k_2 k_3\,[1]\,[2]\,[3]}{k_{-2}}$$

The final equation indicates that the overall order of reaction is three, which is not compatible with the experimental overall order of reaction (=two). In addition, according to this equation, the order of reaction with respect to 2-mercapto-4,6-dimethyl pyrimidine **3** is one, whereas it was actually shown to be equal to zero. For this reason, it appeared that the third step is fast. If we assume that the fourth step (rate constant k_4) is the rate-determining step for the proposed mechanism, in this case, there are two ionic species to consider in the rate-determining step, namely phosphonium ion (I_2) and 2-mercapto-4,6-dimethyl pyrimidine (Z^-). The phosphonium and 2-mercapto-4,6-dimethyl pyrimidine ions, as we have seen in Fig. 12, have full positive and negative charges and form very powerful ion-dipole bonds to the ethyl acetate, the high dielectric constant solvent. However, the transition state for the reaction between two ions carries a dispersed charge, which here is divided between the attacking 2-mercapto-4,6-dimethyl pyrimidine and the phosphonium ions. Bonding of solvent (ethyl acetate) to this dispersed charge would be much weaker than to the concentrated charge of 2-mercapto-4,6-dimethyl pyrimidine and phosphonium ions. The solvent, thus, stabilizes the species ions more than it would the transition state, and therefore E_a would be higher, slowing down the reaction. However, in practice, ethyl acetate speeds up the reaction and for this reason, the fourth step, which is independent of the change in the solvent medium, could not be the rate-determining step. Furthermore, the rate law of formation of the product (fourth step) for a proposed reaction mechanism with application of steady-state assumption can be expressed by

$$\text{Rate} = k_4[I_2][Z^-]$$

By application of steady state for $[I^-]$ and $[Z^-]$, and the replacement of their values in the above-mentioned equation, the following equation is obtained:

$$\text{Rate} = \frac{k_2 k_3\,[1]\,[2]\,[3]}{k_{-2} + k_3\,[3]} \qquad (4)$$

This equation is independent of the rate constant for the fourth step (k_4) and shows why the fourth step would not be affected by a change in the solvent medium. In addition, it has been suggested earlier that the kinetics of ionic species' phenomena (e.g., the fourth step) is very fast [39–41]. If the first step (rate constant k_2) were the rate-determining step, in this case, two reactants (triphenylphosphine **1** and dialkyl acetylenedicarboxylate **2**), as we have seen in Fig. 12, have no charge and could not form strong ion–dipole bonds to the high dielectric constant solvent, ethyl acetate. However, the transition state carries a dispersed charge, which here is divided between the attacking **1** and **2** and, hence, bonding of solvent to this dispersed charge is much stronger than the reactants, which lack charge. The solvent, thus, stabilizes the transition state more than it does the reactants and, therefore, E_a is reduced, which speeds up the reaction. Our experimental results show that the solvent with higher dielectric constant exerts a powerful effect on the rate of reaction (in fact, the first step has the rate constant k_2 in the proposed mechanism), but the opposite occurs with the solvent of lower dielectric constant (see Tables 11–13). The results of the current work (effects of solvent and concentration of compounds) have provided useful evidence for steps 1 (k_2), 3 (k_3), and 4 (k_4) of the reactions between triphenylphosphine **1**, dialkyl acetylenedicarboxylate **2** (**2a, 2b**,

TABLE 12 Values of Overall Second-Order Rate Constant for the Reaction Between **1, 2b**, and **3** in the Presence of Solvents Such As 1,4-Dioxane and Ethyl Acetate, Respectively, at All Temperatures Investigated

		$k_2(M^{-1}\ min^{-1})$			
Solvent	ε	*15.0°C*	*20.0°C*	*25.0°C*	*30.0°C*
1,4-Dioxane	2	417.5	464.3	520.3	599.1
Ethyl acetate	6	641.9	702.6	781.4	876.3

TABLE 13 Values of Overall Second-Order Rate Constant for the Reaction Between **1, 2a**, and **3** in the Presence of Solvents Such As 1,4-Dioxan and Ethyl Acetate, Respectively, at All Temperatures Investigated

		$k_2(M^{-1}\ min^{-1})$			
Solvent	ε	*15.0°C*	*20.0°C*	*25.0°C*	*30.0°C*
1,4-Dioxane	2	483.1	531.3	592.6	660.2
Ethyl acetate	6	706.2	768.1	843.4	917.3

or **2c**), and 2-mercapto-4,6-dimethyl pyrimidine **3**. Two steps involving **3** and **4** are not determining, although the discussed effects, taken altogether, are compatible with the first step (k_2) of the proposed mechanism and would allow it to be the rate-determining step. However, a good kinetic description of the experimental result using a mechanistic scheme based upon the steady-state approximation is frequently taken as evidence of its validity. By application of this, the rate formation of product **4** from the reaction mechanism (Fig. 12) is given by

$$\frac{d[4]}{dt} = \frac{d[\text{ylide}]}{dt} = \text{rate} = k_4\,[I_2]\,[Z^-] \qquad (5)$$

We can apply the steady-state approximation to $[I_1]$ and $[I_2]$:

$$\frac{d[I_1]}{dt} = k_2\,[1]\,[2] - k_{-2}\,[I_1] - k_3\,[I_1]\,[3]$$

$$\frac{d[I_2]}{dt} = k_3\,[I_1]\,[3] - k_4\,[I_2]\,[Z^-]$$

To obtain a suitable expression for $[I_2]$ to put into Eq. (5), we can assume that, after an initial brief period, the concentration of $[I_1]$ and $[I_2]$ achieves a steady state with their rates of formation and rates of disappearance just balanced. Therefore, $d[I_1]/dt$ and $d[I_2]/dt$ are zero and we can obtain expressions for $[I_2]$ and $[I_1]$ as follows:

$$\frac{d[I_2]}{dt} = 0, \qquad [I_2] = \frac{k_3[I_1]\,[3]}{k_4\,[Z^-]} \qquad (6)$$

TABLE 14 Activation Parameters Involving $\Delta G^{\#}$, $\Delta S^{\#}$, and $\Delta H^{\#}$ for the Reactions Between **1, 2a**, and **3, 1, 2b**, and **3** and also **1, 2c**, and **3** at 15.0°C in 1,4-Dioxane on the Basis of the Eyring Equation

Reactions	$\Delta G^{\#}$ *(kJ mol^{-1})*	$\Delta H^{\#}$ *(kJ mol^{-1})*	$\Delta S^{\#}$ *(J mol^{-1}K^{-1})*
1, 2a, and **3**	103	10.4	−321
1, 2b, and **3**	103	12.5	−314
1, 2c, and **3**	107	23.1	−292

$$\frac{d[I_1]}{dt} = 0, \qquad [I_1] = \frac{k_2[1]\,[2]}{k_{-2} + k_3\,[3]} \qquad (7)$$

We can now replace $[I_1]$ in Eq. (6) to obtain the equation

$$[I_2] = \frac{k_2\,k_3\,[1]\,[2]\,[3]}{k_4\,[Z^-]\,\left[k_{-2} + k_3\,[3]\right]}$$

The value of $[I_2]$ can be put into Eq. (5) to obtain the rate Eq. (8) for the proposed mechanism:

$$\text{Rate} = \frac{k_2\,k_3\,k_4\,[1]\,[2]\,[3]\,[Z^-]}{k_4\,[Z^-]\,\left[k_{-2} + k_3\,[3]\right]} \quad \text{or}$$

$$\text{Rate} = \frac{k_2\,k_3\,[1]\,[2]\,[3]}{\left[k_{-2} + k_3\,[3]\right]} \qquad (8)$$

Since experimental data indicated that steps 3 (k_3) and 4 (k_4) are fast but step 1 (k_2) is slow, it is, therefore, reasonable to make the following assumption:

$$k_3\,[3] \gg k_{-2}$$

So the rate equation becomes

$$\text{Rate} = k_2\,[1]\,[2] \qquad (9)$$

This equation, which was obtained from a mechanistic scheme (shown in Fig. 12) by applying the steady-state approximation, is compatible with the results obtained by UV spectrophotometry. With respect to Eq. (9), which shows the overall rate constant (k_2), the activation parameters involving $\Delta G^{\#}$, $\Delta S^{\#}$, and $\Delta H^{\#}$ for three reactions (**1, 2a** and **3, 1, 2b**, and **3**, and also **1, 2c**, and **3**) can now be calculated by using the Eyring equation for the first step (k_2, rate-determining step, Fig. 1) as an elementary reaction; the results are reported in Table 14.

Further Kinetic Investigations

Effect of Structure of Dialkyl Acetylenedicarboxylates. To confirm the above observations, further experiments were performed with diethyl acetylenedicarboxylate **2b** and dimethyl acetylenedicarboxylate **2a**, respectively, under the same

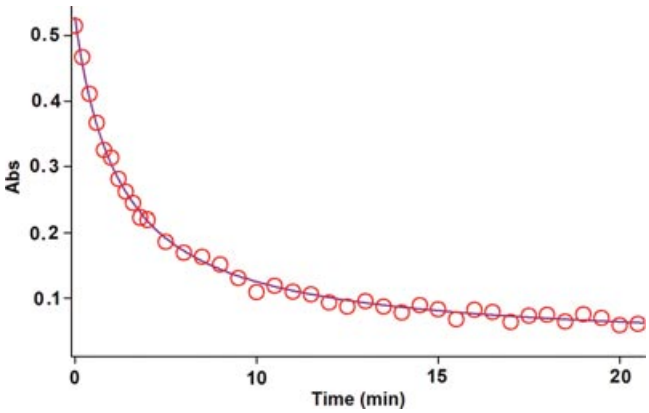

FIGURE 13 Second-order fit curve (solid line) accompanied by the original experimental curve (circles) for the reaction between compounds **1, 2b**, and **3** at 410 nm and 15.0°C in 1,4-dioxane.

conditions as used in the previous experiments. The values of the second-order rate constant (k_2) for the reactions between **1, 2b**, and **3** and **1, 2a**, and **3** are reported in Tables 12 and 13, respectively, for all solvents and temperatures investigated. The original experimental absorbance curves (circles) accompanied by the second-order fitted curves (solid line), which exactly fit experimental curves (circles) (Figs. 13 and 14), confirm the previous observations again for both reactions at 15.0°C and 410 nm.

As can be seen from Tables 12 and 13, the behavior of diethyl acetylenedicarboxylate **2b** and dimethyl acetylenedicarboxylate **2a** is the same for the di-*tert*-butyl acetylenedicarboxylate **2c** (Table 11) with respect to the reaction with triphenylphosphine **1** and 2-mercapto-4,6-dimethyl pyrimidine **3**. The rate of the former reactions was also accelerated in a higher dielectric constant environment and with higher temperatures; however, these rates

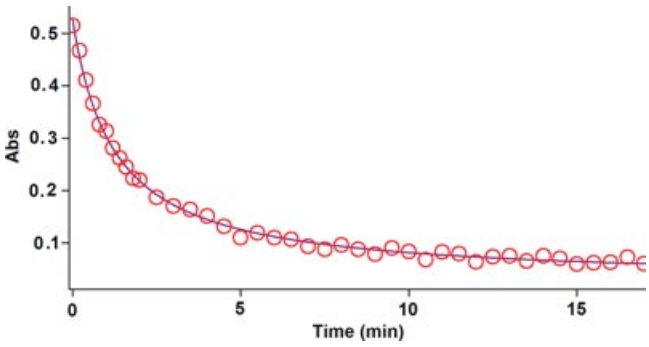

FIGURE 14 Second-order fit curve (solid line) accompanied by the original experimental curve (circles) for the reaction between compounds **1, 2a**, and **3** at 410 nm and 15.0°C in 1,4-dioxane.

under the same condition are approximately 5.5–7.00 times more than for the reaction with di-*tert*-butyl acetylenedicarboxylate **2c** (see Tables 11–13). It seems that both inductive and steric factors for the bulky alkyl groups in **2c** tend to reduce the overall reaction rate (see Eq. (9)). In the case of dimethyl acetylenedicarboxylate **2a**, the lower steric and inductive effects of the dimethyl groups exert a powerful effect on the rate of the reaction.

CONCLUSIONS

The assignment of the *Z*- and *E*-isomers as a minor or major form in both the ylides **4a** and **4c** was undertaken by AIM, NPA methods, and CHelpG keyword. Quantum mechanical calculation clarified how the ylides **4a** and **4c** exist in solution as a mixture of the two geometrical isomers. This result was in good agreement with the experimental data. In addition, the NMR study on the basis of theoretical calculations was employed for determination of chemical shifts and coupling constants of the two major *E*-**4**(**a, c**) and minor *Z*-**4**(**a, c**) geometrical isomers. In addition, kinetic investigation of these reactions was undertaken using UV spectrophotometry. The results can be summarized as follow: (1) The appropriate wavelengths and concentrations were determined to follow the reaction kinetics. (2) The overall reaction order followed second-order kinetics, and the reaction orders with respect to triphenylphosphine, dialkyl acetylenedicarboxylate, and 2-mercapto-4,6-dimethyl pyrimidine were one, one, and zero, respectively. (3) The values of the second-order rate constants of all reactions were calculated automatically with respect to the standard equation, using the software associated with the Cary-300 UV equipment. (**4**) The rates of all reactions were accelerated at higher temperatures. Under the same conditions, the activation energy of the reaction with di-*tert*-butyl acetylenedicarboxylate **2c** (27.9 kJ/mol) was higher than that for the two reactions, which were followed by the diethyl acetylenedicarboxylate **2b** (17.3 kJ/mol) and dimethyl acetylenedicarboxylate **2a** (15.2 kJ/mol) in 1,4-dioxane. (5) The rates of all reactions were increased in solvents of higher dielectric constant, and this can be related to differences in stabilization by the solvent of the reactants and the activated complex in the transition state. (6) Increased steric bulk in the alkyl groups of the dialkyl acetylenedicarboxylates, accompanied by the correspondingly greater inductive effect, reduced the overall reaction rate. (7) With respect to the experimental data, the first step of the proposed mechanism was recognized

as a rate-determining step (k_2) and this was confirmed based upon the steady-state approximation. (8) Also, the third step was identified as a fast step (k_3). (9) The activation parameters involving $\Delta G^{\#}$, $\Delta S^{\#}$, and $\Delta H^{\#}$ were reported for the first step of three reactions.

REFERENCES

[1] Hudson, H. R.; Primary, S.; Tertiary P. In The Chemistry of Organophosphorus Compounds, Hantley, F. R. (Ed.); Wiley: New York, 1990, Vol. 1, p. 386.
[2] Engel, R. Synthesis of Carbon-Phosphorus Bonds; CRC Press: Boca Raton, FL, 1988.
[3] Cadogan, J. I. G. Organophosphorus Reagent in Organic Synthesis; Academic Press: New York, 1979.
[4] Ramazani, A.; Noshiranzadeh, N.; Ghamkhari, A.; Slepokura, K.; Lis, T. Helv Chim Acta 2008, 91, 2252.
[5] Habibi-Khorassani, S. M.; Maghsoodlou, M. T.; Zakarianezhad, M.; Nassiri, M.; Kazemian, M. A.; Karimi, P. Heteroatom Chem 2008, 19, 723.
[6] Maryanoff, B. E.; Reitz, A. B. Chem Rev 1989, 89, 863.
[7] Maghsoodlou, M. T.; Hazeri, N.; Habibi-Khorassani, S. M.; Moeeni, Z.; Marandi, G.; Lashkari, M.; Ghasemzadeh, M.; Bijanzadeh, H. R. J Chem Res 2007, 566.
[8] Anary-Abbasinejad, M.; Anaraki-Ardakani, H.; Hosseini-Mehdiabad, H. Phosphorus Sulfur Silicon Relat Elem 2008, 183, 1440.
[9] Hassanabadi, A.; Anary-Abbasinejad, M.; Dehghan, A. Synth Commun 2009, 39, 132.
[10] Anaraki-Ardakani, H.; Sadeghian, S.; Rastegari, F.; Hassanabadi, A.; Anary-Abbasinejad, M. Synth Commun 2008, 38, 1990.
[11] Yavari, I.; Adib, M.; Jahani-Mogaddam, F.; Sayahi, M. H. Phosphorus Sulfur Silicon Relat Elem 2002, 177, 545.
[12] Okuma, K.; Ishida, T.; Morita, S.; Ohta, H.; Inoue, T. Heteroatom Chem 1995, 6, 265.
[13] Yavari, I.; Zabarjad-Shiraz, N.; Maghsoodlou, M. T.; Hazeri, N. Phosphorus Sulfur Silicon Relat Elem 2002, 177, 759.
[14] Ramazani, A.; Bodaghi, A. Tetrahedron Lett 2000, 41, 567.
[15] Kolodiazhnyi, O. I.; Schmutzler, R. Synlett 2001, 7, 1065.
[16] Wang, Z. G.; Zhang, G. T.; Guzei, I.; Verkade, J. G. J Org Chem 2001, 66(10), 3521.
[17] Soliman, F. M.; El-Kateb, A. A.; Hennawy, I. T.; Abdel-Malek, H. A. Heteroatom Chem 1994, 5, 121.
[18] Abdou, W. M.; El-Khoshnieh, Y. O.; Kamel, A. A. Heteroatom Chem 1999, 10, 481.
[19] Islami, M. R.; Hassani, Z.; Saidi, K. Synth Commun 2003, 33, 65.
[20] Maghsoodlou, M. T.; Heydari, R.; Habibi-Khorassani, S. M.; Rofouei, M. K.; Nassiri, M.; Mosaddegh, E.; Hassankhani, A. J Sulfur Chem 2006, 27, 341.
[21] Yavari, I.; Ahmadian-Rezlighi, L. Phosphorus Sulfur Silicon Relat Elem 2006, 181, 771.
[22] Mahran, M. R.; Abdou, W. M.; AbdEl-Rahman, N. M.; Khidre, M. D. Heteroatom Chem 1992, 3, 93.
[23] Kalantari, M.; Islami, M. R.; Hassani, Z.; Saidi, K. Arkivoc 2006, (x), 55.
[24] Islami, M. R.; Mollazehi, F.; Badiei, A.; Sheibani, H. Arkivoc 2005, (xv), 25.
[25] Maghsoodlou, M. T.; Habibi-Khorassani, S. M.; Rofouei, M. K.; Adhamdoust, S. R.; Nassiri, M. Arkivoc 2006, (xii), 145.
[26] Maghsoodlou, M. T.; Hazeri, N.; Habibi-Khorassani, S. M.; Ghulame Shahzadeh, A.; Nassiri, M. Phosphorus Sulfur Silicon Relat Elem 2006, 181, 913.
[27] Habibi-Khorassani, S. M.; Maghsoodlou, M. T.; Nassiri, M.; Zakarianejad, M.; Fattahi, M. Arkivoc 2006, (xvi), 168.
[28] Kazemian, M. A.; Karimi, P.; Jalili-Milani, F.; Habibi-khorassani, S. M.; Maghsoodlou, M. T.; Ebrahimi, A. Prog React Kinet Mech 2009, 34, 77.
[29] Gebert, A.; Heimgartner, H. Helv Chim Acta 2002, 85, 2073.
[30] Saghatforoush, L.; Maghsoodlou, M. T.; Aminkhani, A.; Marandi, G.; Kabiri, R. J Sulfur Chem 2006, 27, 583.
[31] Reed, A. E.; Weinstock, R. B.; Weinhold, F. J Chem Phys 1985, 83, 735.
[32] Frisch, M. J.; Trucks, G. W.; Schlegel, H. B.; Scuseria, G. E.; Robb, M. A.; Cheeseman, J. R.; Zakrzewski, V. G.; Montgomery, J. A.; Stratmann, R. E.; Burant, J. C.; Dapprich, S.; Millam, J. M.; Daniels, A. D.; Kudin, K. N.; Strain, M. C.; Farkas, O.; Tomasi, J.; Barone, V.; Cossi, M.; Cammi, R.; Mennucci, B.; Pomelli, C.; Adamo, C.; Clifford, S.; Ochterski, J.; Petersson, P. Y.; Ayala, G. A.; Cui, Q.; Morokuma, K.; Malick, D. K.; Rabuck, A. D.; Raghavachari, K.; Foresman, J. B.; Cioslowski, J.; Ortiz, J. V.; Stefanov, B. B.; Liu, G.; Liashenko, A.; Piskorz, P.; Komaromi, I.; Gomperts, R.; Martin, R. L.; Fox, D. J.; Keith, T.; Al-Laham, M. A.; Peng, C. Y.; Nanayakkara, A.; Gonzalez, C.; Challacombe, M.; Gill, P. M. W.; Johnson, B. G.; Chen, W.; Wong, M. W.; Andres, J. L.; Head-Gordon, M.; Replogle, E. S.; Pople, J. A. Gaussian 98, Revision A. 7, Gaussian, Inc., Pittsburgh, PA, 1998.
[33] Bader, R. F. W. Atoms in Molecules a Quantum Theory; Oxford University: New York, 1990.
[34] Biegler-Konig, F. W.; Schonbohm, J.; Bayles, D. J Comput Chem 2001, 22, 545.
[35] Grabowski, S. J. J Mol Struct 2001, 562, 137.
[36] Arnold, W. D.; Oldfield, E. J Am Chem Soc 2000, 122, 12835.
[37] Rozas, I.; Alkorta, I.; Elguero, J. J Am Chem Soc 2000, 122, 11154.
[38] Schwartz, L. M.; Gelb, R. I. Anal Chem 1978, 50, 1592.
[39] Wolff, M. A. Chem Instrum 1976, 5, 59.
[40] Treglon, P. A.; Laurence, G. S. J Sci Instrum 1965, 42, 869.
[41] Okubo, T.; Maeda, Y.; Kitano, H. J Phys Chem 1989, 93, 3721.